Supporting information for:

Understanding the role of surface states on mesoporous NiO films

Lei Tian[a], Robin Tyburski[a], Chenyu Wen[b], Rui Sun[c], Mohamed Abdellah[a,d], Jing Huang[a], Luca D'Amario[a], Gerrit Boschloo[a], Leif Hammarström[a], Haining Tian[a,*]

[a]Department of Chemistry-Ångström Laboratories, Uppsala University, Box 523, SE75120 Uppsala, Sweden.

[b]Department of Electrical Engineering, Uppsala University, Box 534, SE75121 Uppsala, Sweden.

[c]Department of Materials Science and Engineering, Uppsala University, Box 534, SE75120 Uppsala, Sweden.

[d]Department of Chemistry, Qena Faculty of Science, South Valley University, 83523 Qena, Egypt.

Preparation of Ni sol-gel***:*** the Ni sol-gel was prepared based on reported papers[1,2]. In brief, 3 g $NiCl_2$ and 3 g F108 polymer were mixed with 9 g deionized water and 18 g ethanol. Then the mix solution was sonicated overnight (ca. 16 h) resulting in a green and transparent gel. Then, the gel was centrifuged under 10000 rpm/min for 30 min to remove the impurity from the bottom. The resultant gel solution was stored for a week before using. The gel on the top was chosen as Ni sol-gel for the following studies.

ALD Depositions:

Taking NiO mesoporous films as an example, the surface area of the NiO film (1.3 μm) is estimated about 70 m^2/cm^3 in this paper[1]. It means the surface area inside a mesoporous film will be $9.1*10^{-3}$ m^2 with geometric area of 1*1 cm. The size of trimethylaluminum (TMA) should be ca. 6 Ångström in length and it will approximately occupy a surface area of $3.6*10^{-19}$ m^2 ($6*10^{-10}$ $*6*10^{-10}$ m) for a single TMA molecule. Assume a mono-layer adsorption of TMA inside the NiO film, it requires $2.5*10^{16}$ TMA molecules for a 1.3 μm film (91 cm^2). During the ALD, a 0.1 s pulse time (ca. 0.5 mg TMA) is used in ALD Al_2O_3, and it corresponds to ca. $4.2*10^{18}$ TMA molecules in the whole chamber. The area of substrate holder has an approximate diameter of 15 cm, it means the inner surface area of the deposition chamber is about 350 cm^2 (4 NiO samples with 1*1 cm). Therefore, the amount of TMA in one pulse can support ca. 100 NiO films reaching a saturated adsorption.

From the calculation above, this seems both of the ALD procedures are possible to reach a monolayer adsorption. Note that the precursor of TMA needs to diffuse windingly inside a mesoporous film, which means more collisions and longer diffusing distance until reaching a uniformly adsorption. Therefore, the diffusing time needs to be carefully considered, and the

precursor is better to be kept inside the chamber for a longer time before purging directly.

In our previous work, we tried to ALD TiO_2 or ZnO (including Al_2O_3) inside mesoporous NiO. But we found TiO_2 or ZnO more likely localized on the top of the NiO films, which caused that formation of an electronically connected TiO_2 or ZnO layer inside NiO film was problematic[3]. That may be due to that an excess of precursors at each cycle was difficult to be purged away from the NiO. The accumulated precursors reacted with next precursor and blocked the pore on the top of the NiO layer. This could also due to that precursor diffusion was more difficult through the windingly routes in NiO. As a result, the deposition did not reach a monolayer adsorption at each cycle.

Therefore, typical ALD procedures of planer film should be reconsidered when it is applied on a mesoporous film. More attentions should be taken especially only several of ALD cycles. One cycle of ALD should be more careful when applied on a mesoporous films since the precursor adsorption is more easily affected. This can result in diverse situation only due to the possible adsorption of the chamber. Not to say that a mesoporous film over 10 μm in thickness is used.

Films Color:

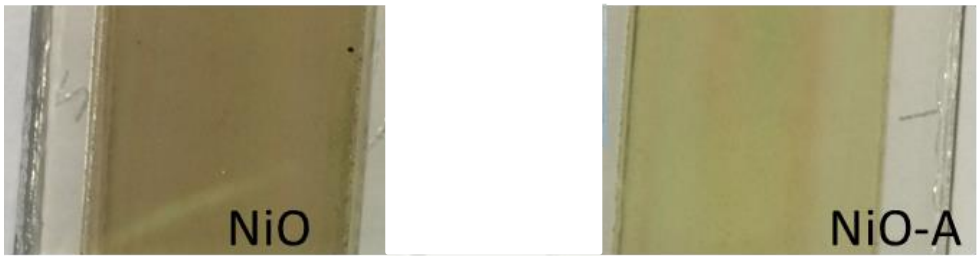

Figure S1. The images of NiO film as prepared (left) and NiO-A film after ALD of Al_2O_3 (right).

UV-vis and Near IR Transmittance Spectroscopy:

Transmittance spectroscopy of the dry film NiO and NiO-A was performed at a Lambda 900 double-beam UV/vis/NIR spectrophotometer (PerkinElmer) with an integrating sphere, and a Spectralon reflectance standard. The scatter and reflection light were carefully subtracted.

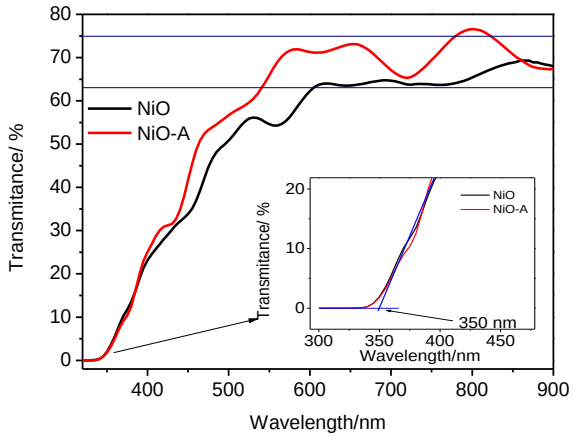

Figure S2. UV/vis/NIR transmittance spectra on the dry films. NiO (black), NiO-A (red).

Crystallization Structure of the NiO and NiO-A Films:

X-ray Diffraction (XRD) was performed in a Siemens D5000 θ−2θ goniometer with CuKα (λ = 1.54051 Å) radiation. XRD measurement with a small angle X-ray irradiation was used to achieve the XRD spectra for the thin films.

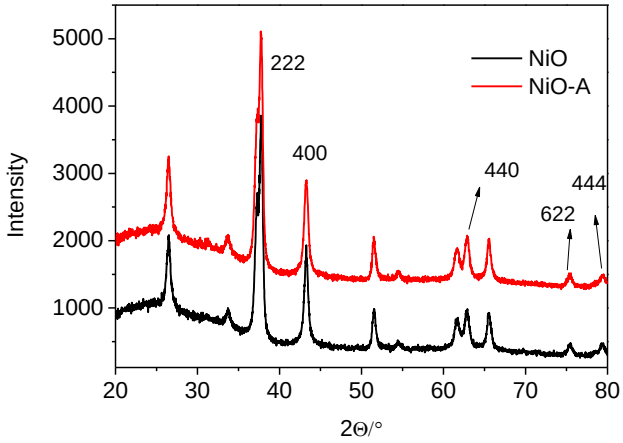

Figure S3 XRD spectra of NiO (black) and NiO-A (red) dry film. The labeled peaks belong to NiO or NiO-A, and the non-labeled peaks belong to FTO glasses.

The Density of States (DOS) of NiO and NiO-A was calculated from the cathodic CV curves. The function of capacitance of NiO and NiO-A on potentials were achieved from equation $C=J_{sc}/v$; J_{sc} is the current density in Figure 1, and v is the scanning rate in CV. $C = \frac{Q}{V} = \frac{J_{sc}t}{V} = \frac{J_{sc}}{V/t} = \frac{J_{sc}}{v}$, in which Q is charge; V is potential. DOS was calculated from the equation of $DOS = C[(1-p)\times e \times l]^{-1}$, $DOS = \frac{C}{e(1-q)l}$, where p is porosity, e is the elementary charge, and l is the film thickness. p is assumed as 0.5 in this paper[4].

X-ray Photoelectron Spectroscopy (XPS) was applied to detect the valence band maximum (VBM) of NiO and NiO-A films.

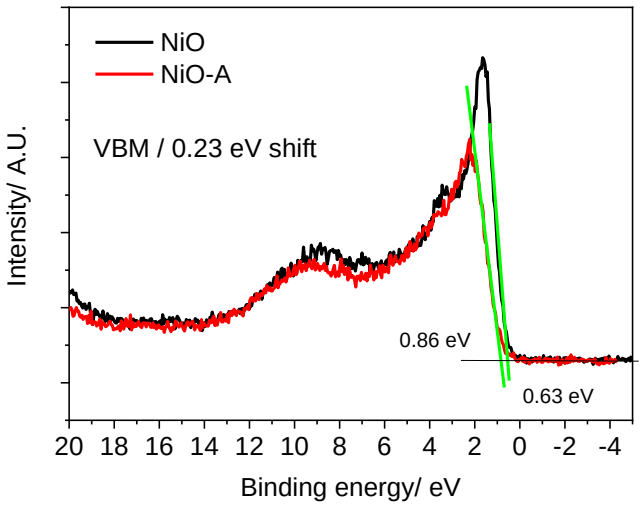

Figure S4. High resolution of XPS spectra (-5 eV to 20 eV) of NiO and NiO-A. The VBM is from the tangent lines in the curves.

Charge Extraction under Open Circuit Condition was performed in NiO and NiO-A based p-DSCs. The details of instrument were described in the main text (transient photocurrent part). For the measurements, the solar cells were kept under open circuit condition. The cells were illuminated for 5s, and then the light was turned off. Meanwhile, the current decay under short-circuit condition was recorded, and the extracted charges was integrated accordingly.

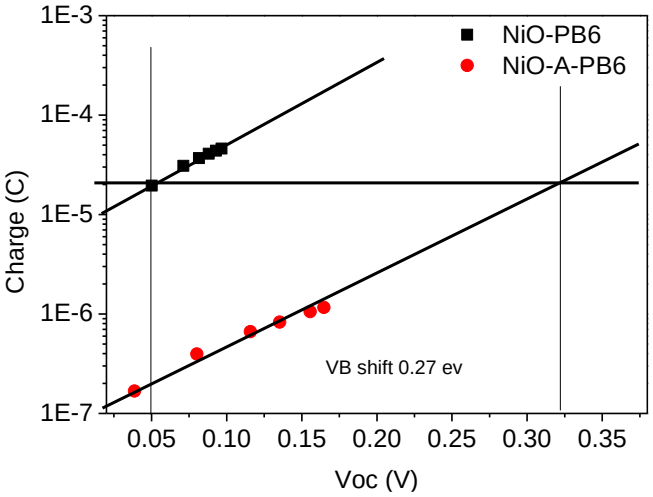

Figure S5. The function of extracted charges on V_{oc} from both NiO and NiO-A based p-DSCs.

If there were no intra bandgap states in both NiO and NiO-A films, extracting same amount of charges will be corresponding to an identical V_{oc}. V_{oc} will be equal to the difference potential of Quasi-Fermi level in NiO or NiO-A and the redox potential (treated as a fixed value). In the Figure S5, the value of V_{oc} was significantly different at a fixed charge extracted. The Quasi-

Fermi level in NiO-A was positively shifted 270 mV compared to that in NiO due to the passivation of the intra bandgap states.

Direct Current (DC) Conductivity Measurement:

In the four-probe resistance measurement, a semiconductor device parameter analyzer (Keysight B1500A, Keysight Technologies, Inc.) was adopted to force the current and measure the voltages with the four source units (SMU, B1517A, Keysight Technologies, Inc.). In order to avoid the stochastic error, the forced current was swept from zero to a certain value (according to the sample resistance). At each current level, the potentials at the two inner electrodes were recorded. Afterwards, the resistance can be extracted by linear fitting the whole potential-current curves. All the electrical measurements were taken in a Faraday cage with the electrical connection through a probe station.

The illumination condition was created by using a white LED lamb (PAR38 module, 17 W, 5000K, Zenaro Lighting GmbH, 420-750 nm) located above the samples ca. 10 cm which is corresponding to a simulated one sun condition at the target wavelength range.

The strips of FTO on the glass were made by etching away those original FTO layers from the white area labeled as 'Glass'. Before etching, the SCOTCH tape in 5 mm width was tapped on the strips of FTO as shown Scheme S1. Then, the rest part of the exposed FTO was cast a thin layer of Zn metal powders. Then, the aqueous solution of 2 M HCl was added on the Zn powders to etch away FTO layer. After etching, the resistance on the glass area should be carefully checked to make sure all the FTO layers have been removed.

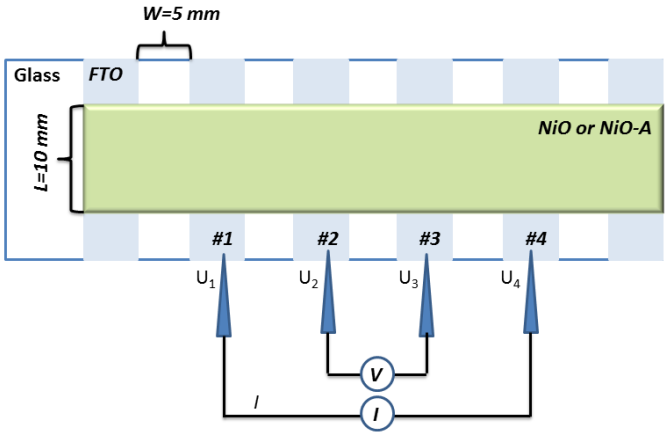

Scheme S1. The NiO or NiO-A samples for resistance measurements with dimension information; and the sketched description of the four-probe resistance measurement.

Table S1. Conductivity of different NiO and NiO-A films or under different conditions.

[a]Samples/condition	Conductivity (S/cm)[a]
NiO	(1.7±0.25)E-4
NiO-A	(2.4±0.27)E-6
NiO-PB6	(4.1±0.46)E-5
NiO-A-PB6	(1.0±0.11)E-6

[b]NiO-PB6 light	(4.1±0.27)E-5
[b]NiO-A-PB6 light	(1.8±0.22)E-6

[a]Each test was repeated three times at least. [b]Dye loading of PB6 is ca. $1.46*10^{20}$ cm^{-3}; Surface states in NiO is ca. $1.95*10^{20}$ cm^{-3}; Surface states in NiO-A is ca. $3.68*10^{19}$ cm^{-3}.

Parameters of Solar Cells:

Table S2. The performance of p-DSC based on NiO and NiO-A film.

	V_{oc} (V)	J_{sc} (mA)	FF	Eff. %	IPCE % (peak)
NiO-PB6	0.105	3.32±0.14	0.34±0.009	0.12±0.008	28±0.86
NiO-A-PB6	0.20±0.009	0.022±0.002	0.41±0.01	0.002±0.0003	< 1%
NiO-PB6-A	0.17±0.003	0.51±0.04	0.46±0.009	0.040±0.003	7.9±0.44

Footnotes: All the solar cell were measured at stimulated AM 1.5 G, 100 $mW \cdot cm^{-2}$ light condition, and active area was 0.25 cm^2 (a black mask of 5*5 mm). The electrolyte is 0.05 M I_2, 0.1 M LiI in acetonitrile. [a]The peak *IPCE* value is added.

Incident Photon-to-Current Efficiency (IPCE) Measurements: *IPCE* was measured by a home-made system with a Xenon light source (Spectral Products ASB-XE-175), a monochromator (Spectral Products CM110) and a Keithley multimeter.

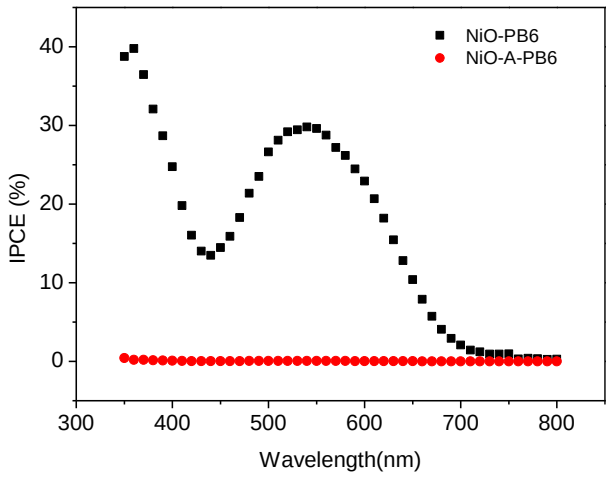

Figure S6. IPCE spectra of NiO and NiO-A based p-DSCs.

Photoelectrochemical Properties of Dye Sensitized NiO and NiO-A film have been investigated. A well-characterized PB6 dyes were used to fabricate NiO-PB6 and NiO-A-PB6 photocathodes. A standard three-electrode electrochemical system was applied, and the properties of NiO-PB6 and NiO-A-PB6 photocathodes were characterized under a linear sweep voltammetry (*LSV*) with chop light (A LED PAR38 module (17 W, 5000K, Zenaro Lighting GmbH, 420-750 nm). From the results in Figure S7, the onset potential of the photocurrent is -

0.02 V and 0.07 V for NiO and NiO-A film, receptively (by assuming the onset potential is at the position where photocurrent density is 0 mA/cm^2). The dark and the light current basically keep constant from -0.2 V to -0.8 V. A clear difference in Figure S7 is that dark and photocurrent density from NiO photocathode are significant larger (ca. 24 times for dark current density, and ca. 20 times for photocurrent density) that of NiO-A photocathode. The experiments clearly show the different photoelectrochemical responses of NiO and NiO-A under dark or light conditions.

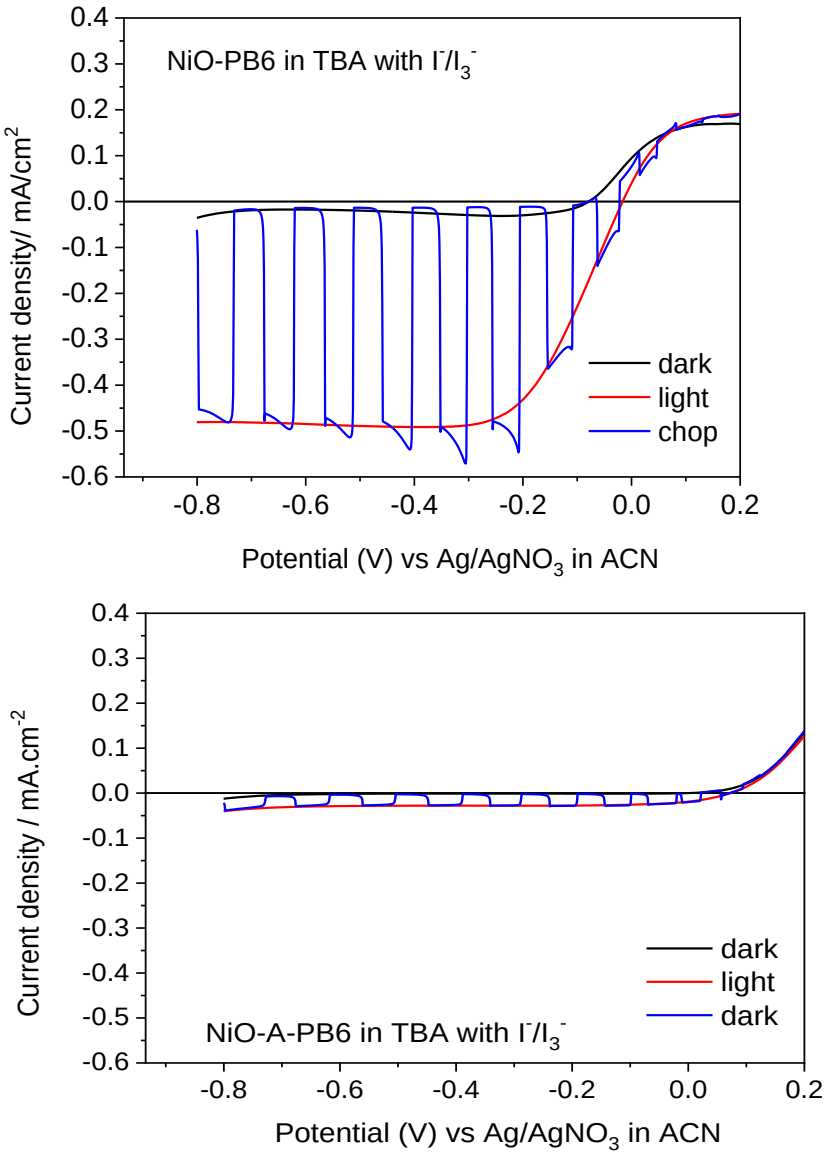

Figure S7. LSV measurements of NiO-PB6 (up) and NiO-A-PB6 (bottom) photoelectrodes collected in 5mM I_2 and 10 mM LiI and 100 mM TBAPF6 in ACN at 5 mV/s scan rate under dark, light and chop light conditions.

CV Measurement with Different Working Electrodes:

The CV measurements were performed inside a glove box (H_2O < 0.1 ppm; O_2 < 0.1 ppm) with

dry ACN solvent and dry supporting electrolyte TBAPF6.

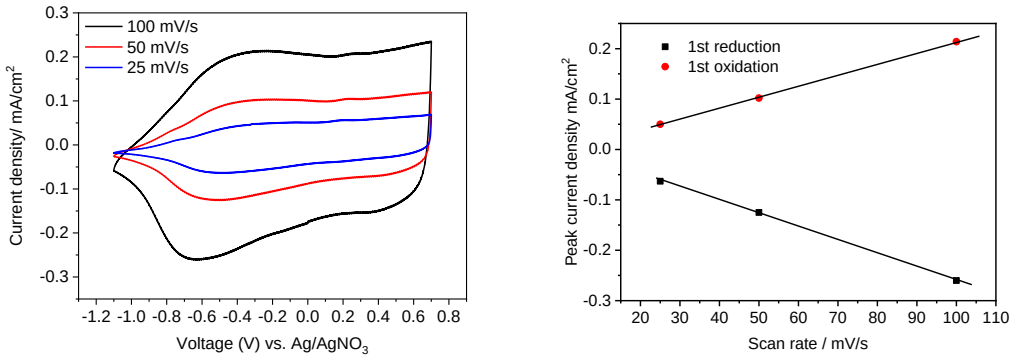

Figure S8. CV of NiO as working electrode collected in 100 mM $TBAPF_6$ in ACN at different scan rates (left); The first redox reaction (ca. -0.5 V in CV (left)): the peak current density *vs.* the scan rate.

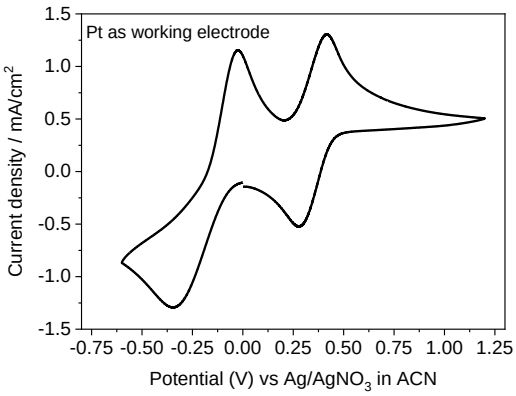

Figure S9. CV of Pt working electrode collected in 5 mM I^-/I_3^- (5mM I_2 and 10 mM LiI) and 100 mM $TBAPF_6$ in ACN at 100 mV/s scan rate.

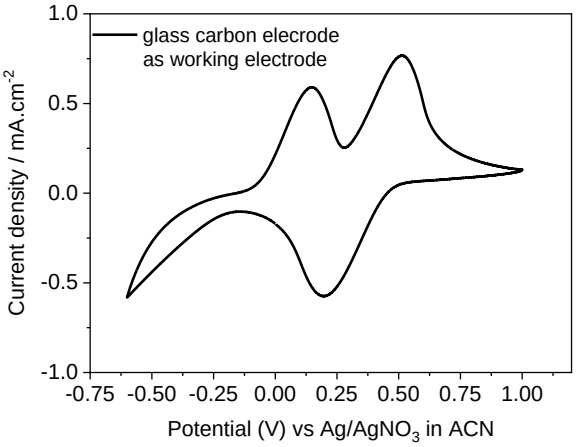

Figure S10. CV of glass carbon working electrode collected in 5 mM I^-/I_3^- (5mM I_2 and 10 mM LiI) and 100 mM $TBAPF_6$ in ACN at 100 mV/s scan rate.

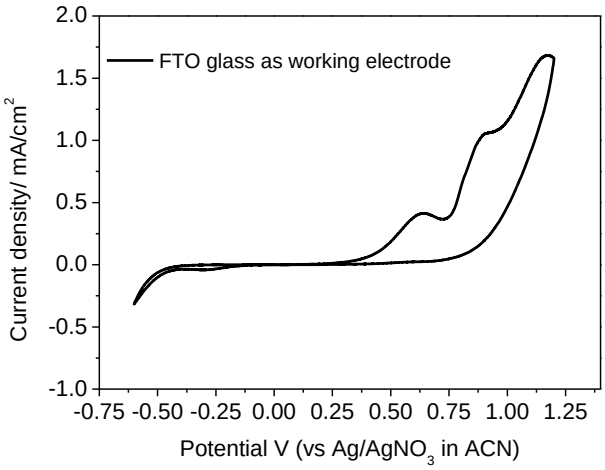

Figure S11. CV of FTO as working electrode collected in 5 mM I^-/I_3^- (5mM I_2 and 10 mM LiI) and 100 mM $TBAPF_6$ in ACN at 100 mV/s scan rate.

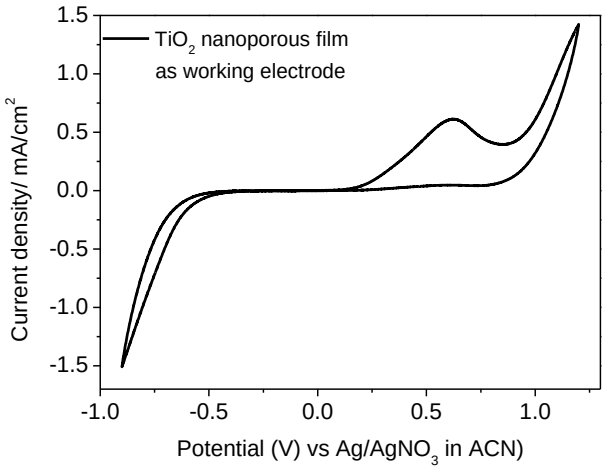

Figure S12. CV of TiO_2 mesoporous film as working electrode collected in 5 mM I^-/I_3^- (5mM I_2 and 10 mM LiI) and 100 mM $TBAPF_6$ in ACN at 100 mV/s scan rate.

Form the CV of TiO_2 in I^-/I_3^-, we did not see the reduction peak around -0.5 V in Figure S12. It is can be explained that there is no DOS in this potential range since there should be inside the bandgap range from -1.0 V to 2.5 V (*vs.* $Ag/AgNO_3$; the edge of CB in TiO_2 is -1.0 V). However, there are significant DOS from -1.0 V to -0.5 V (trap states in TiO_2). Still, no reduction peak can be observed, which should support our conclusion that TiO_2 cannot catalyze I_3^- reduction.

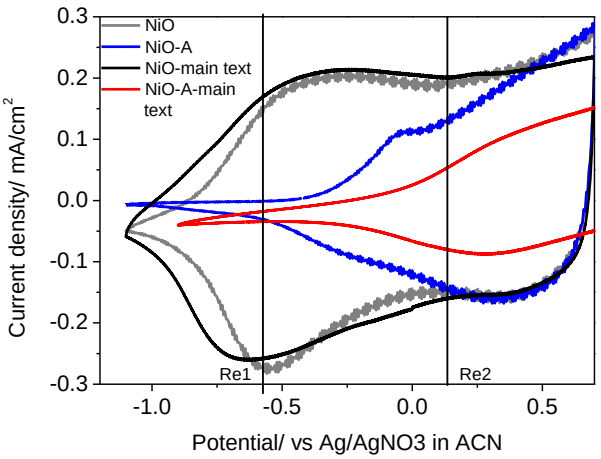

Figure S13. CV of NiO and NiO-A (of some bench of samples) as working electrode collected in 100 mM TBAPF6 in ACN at 100mV/s scanning rate. The CV of NiO and NiO-A are added as comparisons. The black lines at potential of Re1 and Re2 are labeled.

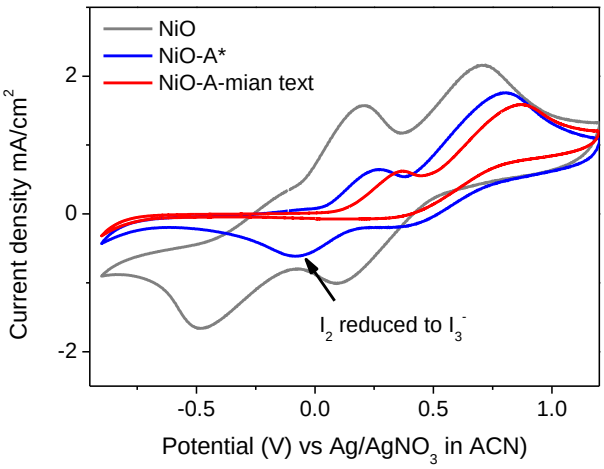

Figure S14. CV of NiO and NiO-A* (of some bench of samples) as working electrode collected in 5 mM I^-/I_3^- (5mM I_2 and 10 mM LiI) and 100 mM TBAPF6 in ACN at 100 mV/s. NiO-A in Figure 5 is added for comparison.

In some bench of samples, we found the surface states cannot be removed in the range of valence band, named as NiO-A*, see Figure S13. The Re2 peak in such sample can be observed at -0.08 V, see Figure S14, is corresponding to (Re2). Combined with the CV in NiO-A in Figure 5, removing parts of the surface states in VB leads to completely loss the Rx2. It probably suggests that those surface states in the valence band range should directly relate to the active sites of catalysis in Re2.

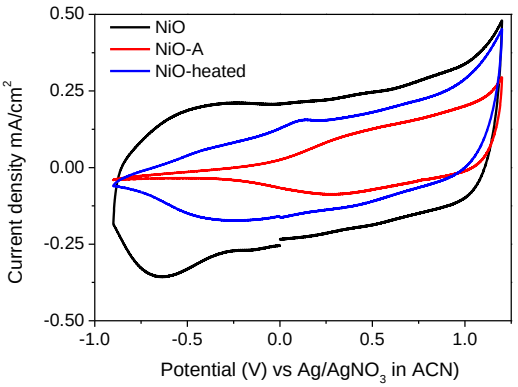

Figure S15. CV of NiO, NiO-A and NiO-heated as working electrodes collected in 100 mM TBAPF6 in ACN at 100 mV/s scan rate.

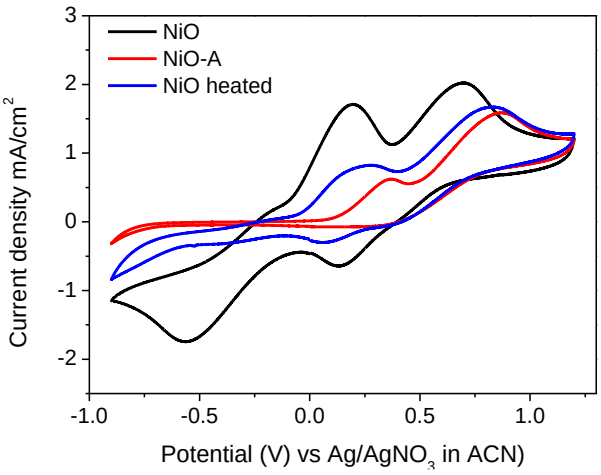

Figure S16. CV of NiO-heat as working electrode collected in 5 mM I^-/I_3^- (5mM I_2 and 10 mM LiI) and 100 mM TBAPF6 in ACN at 100 mV/s. NiO and NiO-A in Figure 5 is added for comparison.

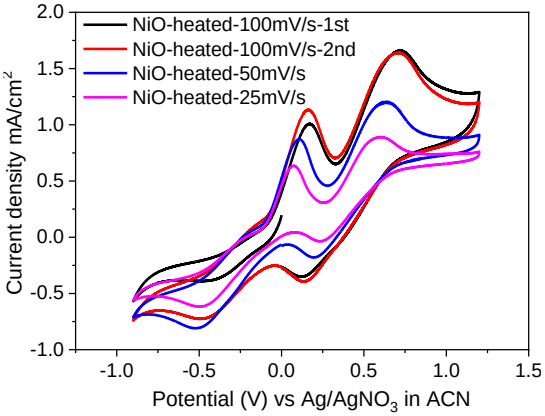

Figure S17. CV of NiO-heated as working electrodes collected in 100 mM TBAPF6 in ACN at scanning rate of 100mV/s, 50 mV/s and 25 mV/s.

Uv-vis Absorption of NiO-PB6 and NiO-A-PB6 were measured at Varian Cary 50. Basically, similar absorption is seen from NiO-PB6 and NiO-A-PB6 films. Light harvested efficiency

(*LHE*) also is calculated by the equation $LHE=1-10^{-A}$ (*A* is adsorption). It shows ca. 70 % LHE (at the peak) can be achieved on both of NiO-PB6 and NiO-A-PB6 films.

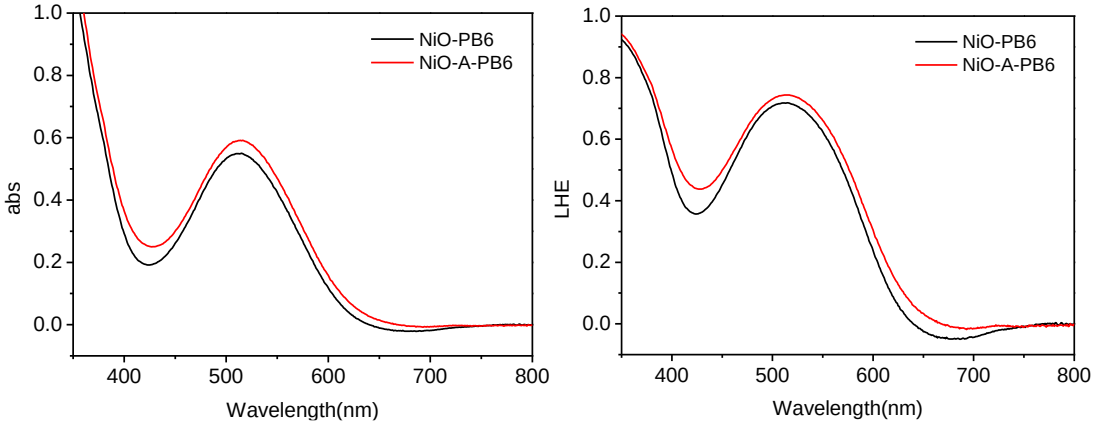

Figure S18. Uv-vis adsorption spectra (left); the calculated LHE vs. wavelength (right).

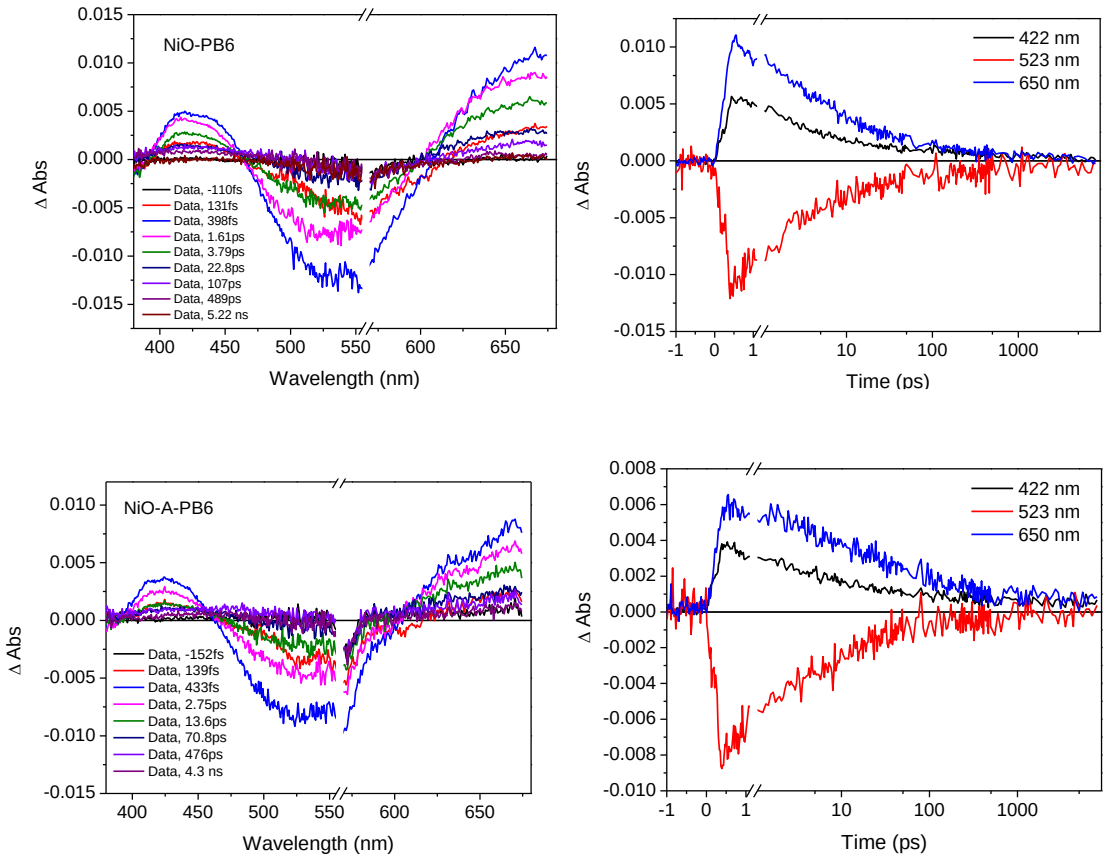

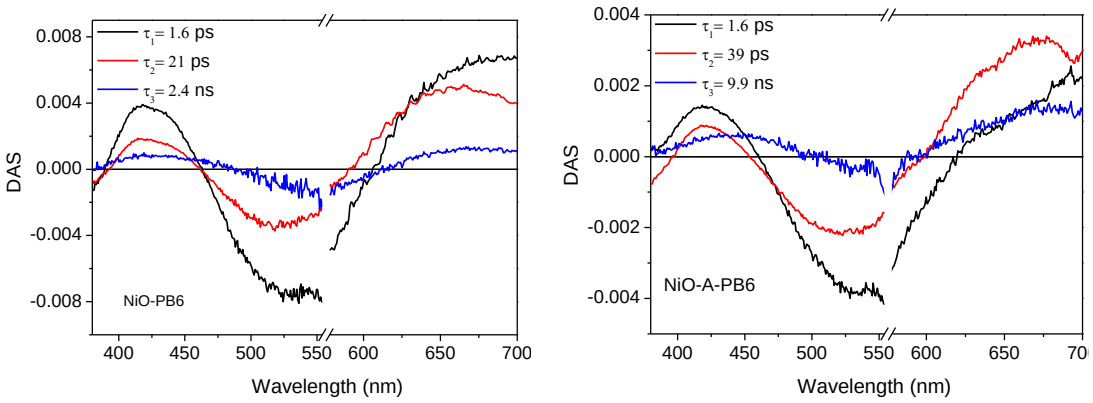

Figure S19. Femtosecond-second transient adsorption spectroscopy (fs-TAS) characterization on NiO-PB6 and NiO-A-PB6. Top two rows: spectra (left); kinetic traces (right); bottom row: decay associated spectra (DAS), fitting with three exponential components.

From the DAS, the signature of reduced PB6 ($PB6^-$) can be observed ca. 650 nm in both NiO-PB6 and NiO-A-PB6 films, matched well with previous reported work. We did not directly observe absorption shoulder of $PB6^-$ from TAS in both NiO-PB6 and NiO-A-PB6 as previous study[5]. The reason is that absorption spectra of excited PB6 (PB6*) and $PB6^-$ are mixed together. However, the black lines in DAS of NiO-PB6 and NiO-A-PB6 films can be reasonably assigned as the component of excited PB6. Both DAS of PB6* show same decay rate constant ($\tau = 1.6$ ps), which means the kinetics of hole injection from PB6*into VB of NiO are identical in both NiO-PB6 and NiO-A-PB6 films. Namely, mono/sub-monolayer of ALD of Al_2O_3 does not affect hole injection, and ALD of Al_2O_3 are basically transparent to electrons (hole injection efficiency can be estimated to unity).

Fitting Details of Figure 6 in Main Text.

The global fitting of multiple wavelengths was performed in software of Glotaran with a triple exponential function after deconvoluting from a Gaussian shaped instrument response function (IRF). The fitted kinetic traces in Figure 6 were from the same global fitting model. The corresponding kinetic parameters were inserted in DAS of Figure S19 (NiO-PB6: τ_1 = 1.6 ps, τ_1 = 21 ps, and τ_3 = 2.4 ns; NiO-A-PB6: τ_1 = 1.6 ps, τ_1 = 39 ps, and τ_3 = 9.9 ns), and the amplitude components can be compared at targeted wavelength (650 nm) in Figure S19. The fitting residual in Figure 6 was given below.

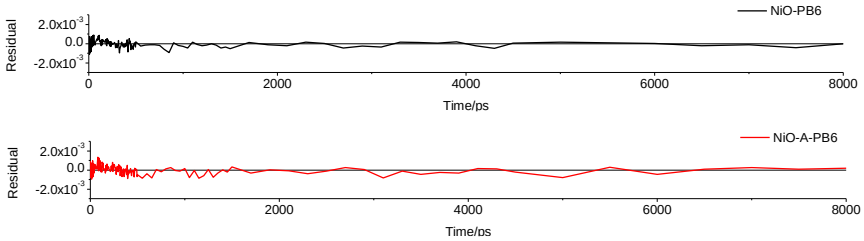

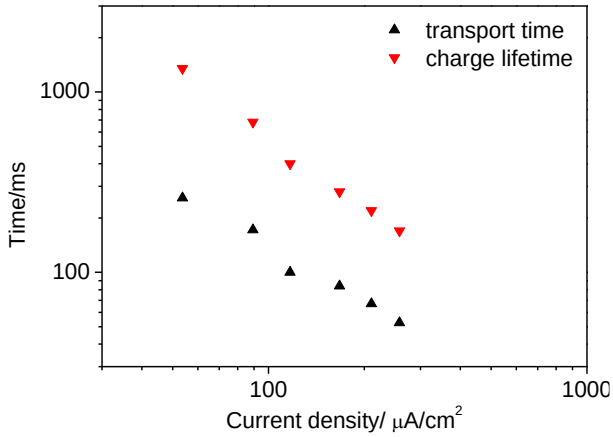

Figure S20. Hole lifetime and transport time on p-DSCs based on NiO-A film.

From hole lifetime (τ_{HL}) and transport time (τ_{HT}), the charge collection efficiency (η_{cc}) is calculated with equation $\eta_{cc}=1-(\tau_{HT}/\tau_{HL})$. Beyond 70% charge collection efficiency (under one sun condition) is obtained on p-DSCs based on NiO-A film.

As known, IPCE can be described as $IPCE = LHE \times \phi_{inj} \times \phi_{reg} \times \phi_{cc}$. The measured IPCE of NiO-A based solar cells is < 1 %. From calculation above, it is reasonable to treat the dye regeneration (<0.02 %; far different from the calculated dye regeneration efficiency in NiO-based p-DSCs[3]) as the performance limiting step in NiO-A based solar cells.

Repeated Experiment of Transport Time (identical as Figure 6).

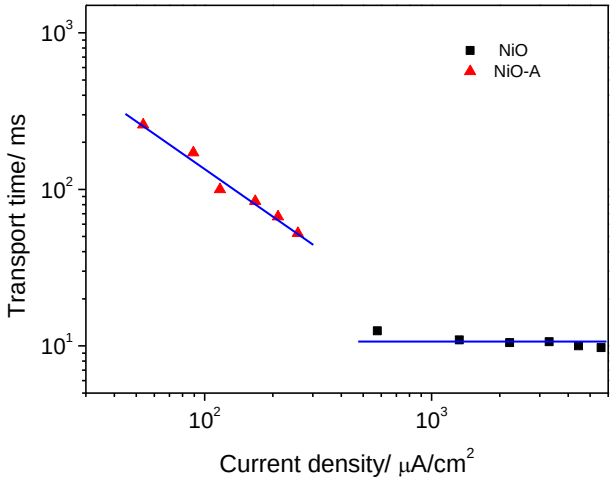

Figure S21. The function of transport time on light intensity (the current density shows linear dependence on light intensity) from NiO and NiO-A based p-DSCs. (exactly same experiment is repeated as Figure 6 and transport time in this Figure S21 is cited from our previous paper[3]).

Conductivity Measurement on nonporous NiO Film: A planar NiO film with thickness of 140 nm was prepared by sputter. The sheet resistance (Four Point Probe, model CMT-SR2000N) is $2.5*10^5$ Ω/sq, conductivity of 0.29 S/cm. Then, a modified one cycle of ALD Al_2O_3 was performed to check the resistance change (named as p-NiO and p-NiO-A).

The clear importance of surface states on NiO film should relate to the characteristic of nanostructure. If the surface states have the tendency to localize on the surface compared to bulk, making it into nanostructure will magnify such effect to many orders of magnitude, due to the larger ratio of surface to volume on mesoporous films. To prove this, a planer NiO film (p-NiO) was prepared by sputtering and corresponding p-NiO-A film by modified one cycle of ALD Al_2O_3. The DC dark conductivity of p-NiO and p-NiO-A is compared, but no conductivity change is found after ALD (both are 0.39 S/cm). This means that there are different conductivity properties of planer and mesoporous NiO films, resulting from the particular nanostructure. The conductivity of single crystal NiO with stoichiometric composition is proved to have significant a high electrical resistance. One theory claims the conductivity of NiO (without perfect stoichiometric composition in reality) results from the presence of Ni^{3+} in the lattice and those Ni^{3+}/holes are tending to delocalize in the lattice which causes the conductivity[6]. With this theory, the Ni^{3+} could be more likely distribute on the surface on NiO, making the conductivity difference on the mesoporous NiO film.

Estimation of the number of surface states per area.

The surface area of NiO film is estimated about 70 m^2/cm^3. The concentration of the surface states in NiO and NiO-A is about $2.78*10^{20}$ cm^{-3} and $8.05*10^{19}$ cm^{-3}, respectively. Thus, 4 surface states is in 1 nm^2 of NiO surface area, and 1 surface state is in 1 nm^2 for NiO-A. In contrast, the trap states in TiO_2 mesoporous film can also be estimated about 1 in 1 nm^2 according to the ref[7]. It supports that the more surface states exist in NiO mesoporous films.

XPS Measurement to Confirm p-NiO.

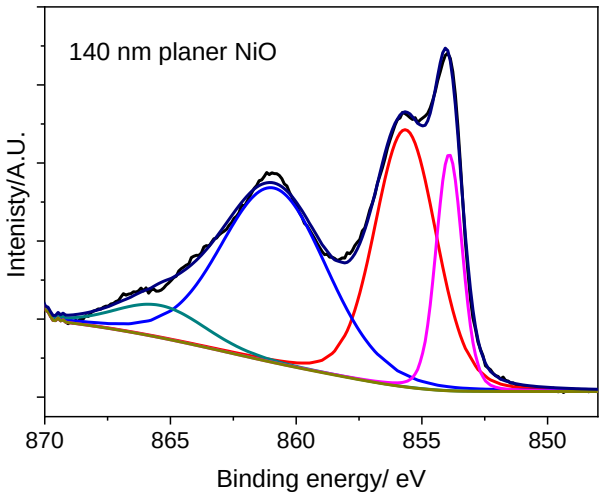

Figure S22. Ni $2p_{3/2}$ spectrum of p-NiO.

XPS Measurement for NiO and NiO-A Films.

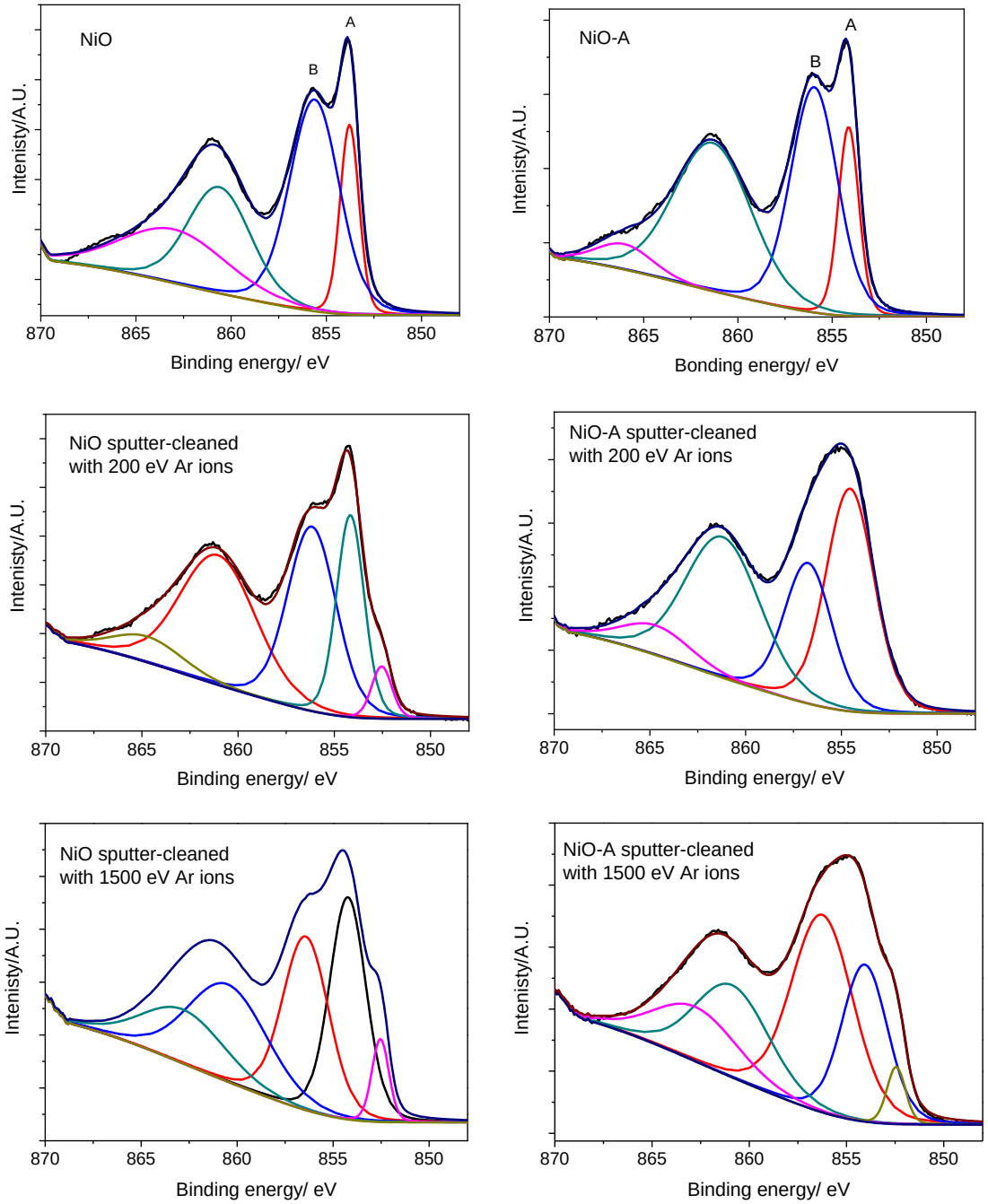

Figure S23. Ni 2p3/2 XPS spectra of NiO and NiO-A film. The films were sputter-cleaned using argon ions for 2 min at 0 eV (top); 200 eV (middle); 1500 eV (bottom). The labeled peaks of A and B are used to compare the difference between the NiO and NiO-A films.

XPS experiments were conducted on a PHI Quantera II scanning XPS microprobe (Chanhassen, NM). The spectra were calibrated against the C 1s peak at 284.8 eV for adventitious carbon.

Table S3. Details parameters of peak A and peak B in Ni $2p_{3/2}$ XPS spectra shown in Figure S23.

Ar ions (eV)	sample	peak A (eV)	peak B (eV)	B:A (peak height)	B:A (peak area)[a]
0	NiO	853.8	855.7	1.07	2.94
	NiO-A	854.2	856.0	1.10	2.72
200	NiO	854.5	856.8	0.97	1.60
	NiO-A	854.2	856.2	0.82	0.63
1500	NiO	854.2	856.5	0.99	0.99
	NiO-A	854.1	856.3	1.14	1.69
[b]Planer NiO film					
-	p-NiO	853.9	855.7	1.05	2.55

[a]The peak area is integrated. [b]XPS of p-NiO is added for comparison.

To further understand the properties of the surface states on NiO, XPS was performed. The underlying chemical nature of surface state of NiO has been investigated by many groups[8,9], and it is commonly characterized by XPS due to its sensitivity to the surface. However, the reported results are controversial and ambiguous, especially for the indication of Ni oxidation states in Ni $2p_{3/2}$ XPS spectrum. Here, we do not try to assign a XPS peak to a corresponding Ni oxidation state. XPS measurements are applied to prove that the typical surface feature of NiO is still kept in NiO-A, as confirmed in Figure S23 [the overall Ni 2p3/2 XPS spectra are changed in which peak A and B is merged together in the spectrum of NiO-A, and the area ratio of B:A is very different (1.6 for NiO, 0.63 for NiO-A)]. In the XPS measurements, Ar ions with relatively low energy are commonly used to clean the surface of samples. It has been also reported that metal oxides could be reduced by the Ar ions if the energy is significantly high[10]. Interestingly, from our sputter-cleaning measurements with Ar ions (Figure S23 middle), we are able to observe a clear Ni metal peak (around 852.5 eV) formed in NiO, but not in NiO-A (see discussion below). This suggests that the surface states on NiO are easier to be reduced than that on NiO-A.

Form XPS studies in NiO film, we know the peak A is belong to Ni^{2+} state. However, the explanation for the shoulder of peak B is controversial. The peaks B is known really sensitive to the change of surface states. Here, we do not try to assign peak B to any Ni oxidation states. A confident conclusion here is the surface states in NiO is more reductively active than the surface states in NiO-A.

Photoelectrochemical Properties of Dye sensitized NiO and NiO-A in acetate buffers with different pH. LSV measurements are similar as Figure S7 except that an Ag/AgCl reference electrode (in 3M NaCl) was used.

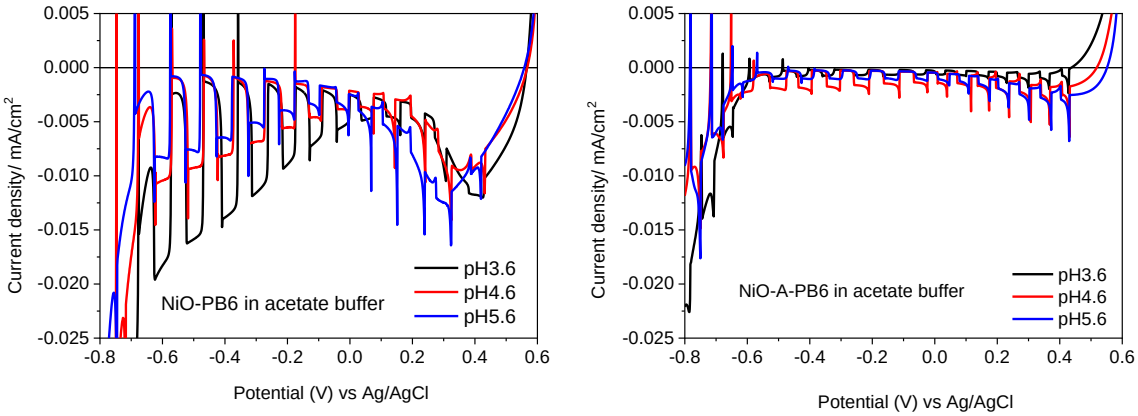

Figure S24. LSV measurements (Ag/AgCl/3.0 M NaCl reference electrode) of NiO-PB6 and NiO-A-PB6 photoelectrodes collected in 50 mM acetate buffer with different pH at 5mV/s, under dark, light and chop light conditions.

Reference:

(1) Sumikura, S.; Mori, S.; Shimizu, S.; Usami, H.; Suzuki, E. Syntheses of NiO nanoporous films using nonionic triblock co-polymer templates and their application to photo-cathodes of p-type dye-sensitized solar cells. *Journal of Photochemistry and Photobiology A: Chemistry* **2008**, *199*, 1-7.

(2) D'Amario, L.; Antila, L. J.; Pettersson Rimgard, B.; Boschloo, G.; Hammarström, L. Kinetic evidence of two pathways for charge recombination in NiO-based dye-sensitized solar cells. *The journal of physical chemistry letters* **2015**, *6*, 779-783.

(3) Tian, L.; Törndahl, T.; Lin, J.; Pati, P. B.; Zhang, Z.; Kubart, T.; Hao, Y.; Sun, J.; Boschloo, G.; Tian, H. Mechanistic Insights into Solid-State p-Type Dye-Sensitized Solar Cells. *The Journal of Physical Chemistry C* **2019**, *123*, 26151-26160.

(4) Flynn, C. J.; McCullough, S. M.; Oh, E.; Li, L.; Mercado, C. C.; Farnum, B. H.; Li, W.; Donley, C. L.; You, W.; Nozik, A. J. Site-selective passivation of defects in NiO solar photocathodes by targeted atomic deposition. *ACS applied materials & interfaces* **2016**, *8*, 4754-4761.

(5) Tian, L.; Föhlinger, J.; Pati, P. B.; Zhang, Z.; Lin, J.; Yang, W.; Johansson, M.; Kubart, T.; Sun, J.; Boschloo, G. Ultrafast dye regeneration in a core–shell NiO–dye–TiO2 mesoporous film. *Physical Chemistry Chemical Physics* **2017**, *20*, 36-40.

(6) Yamashita, J.; Kurosawa, T. On electronic current in NiO. *Journal of Physics and Chemistry of Solids* **1958**, *5*, 34-43.

(7) Nelson, J.; Eppler, A. M.; Ballard, I. M. Photoconductivity and charge trapping in porous nanocrystalline titanium dioxide. *Journal of photochemistry and photobiology A: Chemistry* **2002**, *148*, 25-31.

(8) Marrani, A. G.; Novelli, V.; Sheehan, S.; Dowling, D. P.; Dini, D. Probing the redox states at the surface of electroactive nanoporous NiO thin films. *ACS applied materials & interfaces* **2013**, *6*, 143-152.

(9) Grosvenor, A. P.; Biesinger, M. C.; Smart, R. S. C.; McIntyre, N. S. New interpretations of XPS spectra of nickel metal and oxides. *Surface Science* **2006**, *600*, 1771-1779.

(10) Kim, K.; Winograd, N. X-ray photoelectron spectroscopic studies of nickel-oxygen surfaces

using oxygen and argon ion-bombardment. *Surface Science* **1974**, *43*, 625-643.